ISSN: 2978-3801

Journal of Global Warming and Climate Change

SCIENTIFIC Research and Community

Research Article

Open Access

A Global Predictive Climate Model

Éric Zeltz

Route du Moulin 05500 La Motte en Champsaur, France

ABSTRACT

Objective: The main objective of the work presented in this article was to obtain a global climate model capable of providing reliable forecasts until 2100 regarding the most Important global parameters of the climate system: atmospheric temperature, ocean temperature, cloud cover, atmospheric albedo, subsidence of the oceanic mixed layer and, finally, oceanic stratification. This, while taking into account the different scenarios defined by the IPCC concerning GHG emissions for the period 2025-2100.

Methods: To achieve this objective, the choice was made to use a discrete model whose implied relationships directly aim to obtain the monthly average global results of the studied parameters, without going through the lower scales. Thus, the difficulties related to the strong non-linearity encountered in most phenomena at lower scales largely disappear and make the model much more deterministic than stochastic, unlike the much more complex GCMs developed by the major climate institutes. The model in question is structured from a recent earlier version (2024) developed by the authors.

Results

The main results obtained from this modeling are as follows:

- The radiation budget has been declining since the beginning of the period considered (1955-2100). The radiative forcing is decreasing and tends towards 0.
- The results vary very little, regardless of the GHG emissions scenarios considered. For the four scenarios considered, the increase in atmospheric temperature over the period 1955-2100 will be approximately 1.8 ± 0.4°C (95% confidence level).
- Ergodicity and thermodynamic equilibrium of the current climate system.

Conclusion: To break the thermodynamic equilibrium of the current global climate system and return to a new equilibrium with a cooling trend, we must return to CO_2 emissions below 300 ppm (assuming that other GHGs follow a corresponding decline).

***Corresponding author**

Éric Zeltz, Route du Moulin 05500 La Motte en Champsaur, France. E-mail: ericzeltz@wanadoo.fr

Received: April 15, 2025; **Accepted:** April 21, 2025; **Published:** April 30, 2025

Keywords: Climate Modeling, Ergodicity, Thermodynamic Equilibrium, Radiative Forcing

Introduction

In particular because of the ongoing climate changes, the consequences of which must be anticipated on the ecosystem, most of the major international climate institutes have developed global climate models (GCMs) capable of delivering increasingly detailed and detailed simulations of the future global climate. In these models, the virtual geographical space is composed of "meshes" in which the equations and parameterizations necessary for the modeling of the climatic variables at play are written. The interactions between cells are themselves defined mathematically. Among other assumptions that they must be able to take into account, these models are designed in such a way that they can consider the main possible scenarios for greenhouse gas emissions and more generally for future anthropogenic influences.

It is clear that the finer the mesh, the more accurate the model will be and therefore the more successful the simulations obtained will be. And besides, the resolution is still insufficient to directly reach certain important phenomena such as the evolution of cloudiness or the dynamic and thermodynamic configurations associated with phenomena such as Severe Convective Storms (SCS), mesoscale systems, etc. From this point of view, we therefore need not only these full complexity models, but also ideally a further increase in resolution.

That said, due to the strong non-linearity of the phenomena involved, these models are much more stochastic than deterministic. This comes from an observation first made by Henri Poincaré: in this type of phenomenon, the slightest deviation in the initial conditions, the slightest disturbance, the slightest rounding error in the calculations can be amplified and prevent any long-term forecast [1]. It was also on a non-linear model linked to the climate that Poincaré's intuition was definitively confirmed in 1963 by Edward Lorenz [2]. Since most of the phenomena that occur in the climate have this chaotic aspect, the planet's climate system is itself a chaotic system. More precisely, it is a dissipative chaotic system (in thermal disequilibrium) composed of interacting elements and powered almost entirely by solar radiation [3].

Mathematically, the process can be perfectly deterministic by the equations that model it; but physically, over a sufficiently long period of time, it seems unpredictable, "chaotic". This is called chaotic determinism. It follows that the simulations provided by the GCMs cannot claim to come close to future reality, no matter how fine their resolution may be. And further progress made for the latter will not necessarily increase the realism of the simulations obtained because it has been known for a long time that a fine spatial scale explicitly taken into account can also generate errors.

On the other hand, several simulations obtained from such a model by taking different initial conditions can make it possible to distinguish the variations resulting from the natural variability of the climate from those resulting from a particular phenomenon such as that of forcing caused by greenhouse gases (GHGs), El Niño-Southern Oscillation (ENSO), Ocean Surface Temperature (TSO), the Intertropical Convergence Zone (ITCZ), or other important climatic phenomena. But it will then be all the more necessary to simulate as "the forced theoretical portion is small. For example, the detection of the atmospheric signal in the tropical Pacific forced by ENSO is detectable from 3 simulations. The detection of the atmospheric signal forced by the TSOs over the North Atlantic requires at least 25-30 simulations" [3]. And obtaining just one of these simulations requires a lot of computing power and a lot of time.

So, in addition to these last two very strong constraints, if high-resolution GCMs are useful, they also have major and practically insurmountable flaws because they are inherent to the chaotic side of the climate system: unless by pure chance, their simulations will not be able to realistically deliver the future evolution of the main climate parameters such as the average temperature of the atmosphere on the ground, that of the Upper Oceanic Stratum (UOS), the average evolution of cloudiness, etc., i.e. what essentially determines the future climate of the globe and which current political and economic decision-makers must know as well as possible.

In this work, we present a discrete model, much less complex in its design than GCMs, but unlike them, largely deterministic and non-stochastic. It will therefore be able to deliver real forecasts on the main global average parameters that define the climate.

It is based on relationships obtained for the most part using a new method of studying climate time series: the method of average lengths, or simply "MAL"[4].This method makes it possible to highlight and specify correlations between the climatic entities at play and then to obtain relationships that capture the average interactions between them. And since each climatic entity is influenced by the average of other entities, the system thus obtained can be included in the framework of mean field theory [5,6]. The model thus built will be able to deliver real long-term forecasts, and not simple trends built on stochastic, as GCMs do.

The Plan for this Work is as Follows:

Section 2: A Priori Justifications of the Determinism of the Model

- We begin by justifying what may seem like a paradox, namely that from a system as chaotic as the climate system, we can build a deterministic model for the main global mean parameters. We will give different points of view showing that determinism can arise from a system that is nevertheless chaotic: that of mathematics, that of the physical sciences. Then, in Section, we describe the approach adopted and what makes it original compared to the GCMs.

Section 3: Presentation of the Model

- After describing the objectives and the assumptions taken into account by the model, we detail and explain the mathematical relationships used. Finally, we show how possible GHG emission scenarios are considered

Section 4: Study of the Model

- We start by giving the "theoretical" variations of the modeled parameters and then their asymptotic behaviour. We describe there the model's projected evolution of the radiation budget and its forcing. In section, we test the main constants of the model and then interpret these tests.Then we give examples of simulations obtained. Then, we study the consistency of the model with what is known for the period preceding that of the study (1955-2100). Finally, we show that what is delivered by the model is in agreement with an ergodicity hypothesis about the climate system.

Section 5: Conclusion

- Given the model's predictions and the consequences to which it leads, we indicate what we believe to be the approach to follow if we want to regain a climate that is fully beneficial to the ecosystem and therefore to humanity.

A Priori Justifications of the Determinism of the Model

Mathematics Perspective

We will give here several mathematical situations that show that large-scale determinism can arise from a dynamical system that is nevertheless chaotic at the level of small scales:

- First in the theory of "mean field limits" [5,6]. In this study, we can look at a stochastic process describing a typical particle (e.g. subject to Brownian motion) and deduce the statistical behavior of the set of N particles as N approaches infinity. The terminology "limits of mean fields" comes from the fact that the action of each particle in the system of N particles becomes smaller and smaller as $N \to \infty$, but the average action of the particles is of order 1. By crossing the limit from a chaotic model of the Brownian motion of particles, we were able to find the Boltzmann equation which describes the macroscopic statistical behavior of a thermodynamic system outside the state of equilibrium [6]. Other examples of the same type are given in Vilani and Mischler [5,6]. This shows that from a system that is nevertheless very chaotic on a small scale can emerge a large-scale deterministic model.

- Even if a priori the ergodic hypothesis is very difficult to verify, all the more so for a system as complicated as that of climate, it can be realized [7]. In this case, the system tends, in the various possible senses of the calculation of probabilities, towards a limit state independent of the initial situation [8]. This allows us to envisage that the "limit model" (that of the averages of the climate parameters at stake) is not purely chaotic, but on more or less long time scales becomes deterministic, like the one we propose for the global climate system.
- Moreover, in the context of chaos theory some dynamical systems have strange attractors, where the system repeatedly explores a set of states [9]. If the climate system has such an attractor, it could indicate a form of ergodicity.

Physical Science Perspective

The climate system is chaotic in the mathematical sense of the term: no matter how precise and elaborate the mathematics of the model may be, it will not be able to "follow" the reality of the climate for more than a few days or weeks. But it is not mathematics that makes physical reality. In the expression "chaotic determinism" that qualifies the climate system, there is the word "determinism". The physical reality concerning the climate is entirely determined: if on such a day there is or will be a thunderstorm in such and such a place, it is because all previous and related conditions must have led to that thunderstorm at that time and place. And the famous butterfly wing that beats 10,000 km further is part of this anteriority and this environment, but exactly like the rest, and probably with infinitely less direct responsibility than, for example, an increase in heat that raged at the place where the storm took place. Moreover, it has been known for several years that this "butterfly effect" in the original sense of the term has no chance of playing a role 10,000 km further away because it blends completely into the local climate system long before it can play any role for the storm in question [10]. Also, from the point of view of the physical sciences, nothing a priori can prevent the global averages of the main parameters that make up the climate from obeying determined and determining laws. This is even if they are the averages of physical quantities that seem chaotic.

This is what we see in fluid mechanics. For example, in an experiment described by Nicoud and which consisted of making speed measurements in a pipe subjected to a high-flow wind tunnel [11]. In Figure 1, the graphs on the left represent two series of speed measurements recorded over time in this pipe, for identical durations. This experiment clearly shows that the speed signal measured at the same location in the same wind tunnel is not reproducible. It illustrates the chaotic nature of such flows. However, in the graphs on the right, we can see that the velocity distribution is Gaussian and that the average velocities and standard deviations are identical for the two experiments. So as remarked Nicoud, "Is the probability density of speed signals reproducible, or deterministic. The signals are therefore different but they share the same statistical moments (mean, variance, etc.) [11]."

In a much more global way, the Earth system (i.e. planet and atmosphere) is subject to the laws of thermodynamics, in particular to its second law. This requires that closed systems tend towards a state of equilibrium in the long term. The Earth system is almost closed in terms of masses and it receives a permanent supply of energy from the sun. So even if it undergoes significant disturbances in the short or medium term (variations in solar activity, volcanic eruptions, GHG emissions, aerosol impact, etc.), on longer time scales, the system can regain and maintain a certain thermal equilibrium. This goes in the direction of a form of ergodicity, in the sense defined in the previous section.

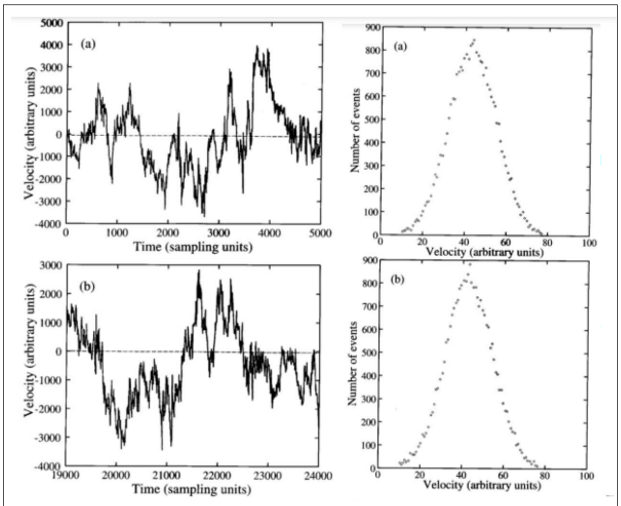

Figure 1: On the left, Two Examples of Changes in Speeds Recorded over Time in a Pipe Subjected to the same wind Tunnel for Identical Durations. On the Right, the Corresponding Histograms of the Speed Distributions. Adapted from Nicoud [11].

Approach and Comparison with GCMs

Although the climate system is chaotic, the different situations and points of view presented in the two previous sections combine to show that the achievement by an adapted model of the major average global parameters of the climate is conceivable. If statistical characteristics such as global averages are preserved by chaos, it is only these characteristics that a climate model that claims to be predictive must strive to obtain. To do this, the interactions between the different important parameters that make up the climate must be analyzed, and not through what happens locally, as the GCMs do, but directly and globally. We therefore need a method of analysis that allows it. This method exists, it is the MAL which makes it possible to detect precise signals of interactions from time series of climate data. It is set out in detail in Zeltz [4]. This preliminary analysis work is described in three previous articles and is the basis of the model presented [12-14]. Here is a quick summary of the different stages of its design and some elements of comparison with GCMs:

- The interactions identified by the MAL are translated into "mean field" relationships that represent the average effects of the components on the overall climate system. Each of the recurrence relations thus obtained and giving the evolution of a given average climatic parameter captures as best as possible the average effect that the other parameters have on it.
- The model also takes into account the average effects that GHGs will have on the parameters, by being able to modify the possible scenarios.
- The constants in play are calibrated using historical data.
- Natural variability is taken into account by random coefficients, the only stochastic part of the model.
- The basic model is associated with its "theoretical" model, i.e. for which these random coefficients have been removed. The simulations obtained through it make it possible to precisely reach the trends on the various simulated parameters.
- The model is self-sustaining, in the sense that it does not seek to follow presupposed trends and has never been corrected or rectified to take into account what the GCMs obtain, for example.
- The model makes it possible to generate simulations very quickly with a simple microcomputer. And thus to easily obtain the confidence intervals of each of the simulated parameters. Unlike GCMs who have such computational complexity that such an approach is practically impossible with them.
- GCMs take into account a multitude of variables and interactions, at all scales, either directly or through parameterization. This increases the sources of uncertainty tenfold. On the other hand, the model presented simplifies these interactions, which mechanically can reduce uncertainties.

Of course, natural variability (which is not chaos) intervenes and therefore the predictivity of the model can never be absolute: such a fortuitous volcanic eruption, such an El Ninô event that is difficult to predict, etc., can have significant repercussions on the global mean parameters and therefore uncertainties will remain on the predictions given by the model. Moreover, this mean-field approach to the model is an approximation that may not capture all the details of complex interactions in the climate system. Another important reservation for the predictivity of the model presented here is that the answer given by the model cannot be uniform, since it will depend on the scenarios that can be envisaged, particularly concerning greenhouse gas emissions of anthropogenic origin.

But unlike GCMs, the predictions made by the model will be expurgated as much as possible of the chaotic part that goes into climate modeling. It is therefore in this sense that we assert that the model presented here is more predictive than stochastic. A climatologist from the Pierre-Simon Laplace Institute (IPSL) in a lecture given at the Collège de France on January 9, 2025 and entitled "Are climate models reliable?" answers this question in the negative [15]. This response concerned the IPSL model and the other GCMs of the major international climate institutes. This is not our answer to the model presented here.

Presentation of the Model

Objectives

The main objectives of the model presented are as follows:

- To reach directly (i.e. without going through small scales) the average changes up to 2100 of five major climate parameters: 1- The atmospheric temperature at the bottom of the troposphere. 2- That of the Upper Oceanic Stratum (UOS) which we assimilate to the mixing layer located above the thermocline. 3- Cloud cover. 4- Oceanic stratification 5- Sinking of the mixing layer.
- To be able to deliver simulations of these five parameters by placing themselves in the main scenarios used by the Intergovernmental Panel on Climate Change (IPCC) concerning greenhouse gas (GHG) evolutions.

The fact that we did not use small scales led us to choose very simplifying hypotheses on the environments involved (atmosphere, oceans, land, ice, etc.) or on the consideration of various dynamics (currents, winds, precipitation, cloud movements, etc.). We briefly present them in the following two sections.

Hypotheses about the Environments in Play

The seas and oceans are the majority since they cover approximately 70% of the surface of the terrestrial globe, but their role in the calorific balance of the Earth is even more important than this percentage would suggest. For example, according to Levitus et al, they absorb about 93% of the additional heat since 1955, the rest being shared between the continents, the ice and the atmosphere [16,17].

Also, to build our model, we consider that the impact of the continents and the ice does not essentially modify the global energy balance.

Hypotheses on the Dynamics

As can be seen, for example, in a mountain stream, the movements of the fluids introduce an essential variable: for an identical heat input in a given volume, the higher the circulation of the fresh fluid arriving there, the less rapid the rise in temperature in the volume in question will be. This applies to the water in the mixing layer, which is constantly stirred by multiple currents and whose surface is agitated by the winds. This also applies to the lower atmosphere, which is itself in perpetual motion because of winds such as trade winds caused by the rotation of the Earth, and also by vertical convection caused by differences in density or atmospheric pressure. On the other hand, the UOS is in contact with an increasingly cold zone (the thermocline). Similarly, the troposphere, which cools very quickly with altitude (around -6.5°C per km), is topped by the very cold base of the stratosphere (about -55°C). This proximity to cold or very cold areas has a huge impact on both environments and means that the intensive mixing of all origins that takes place there is at least as much influenced by these cold areas as by the heat of solar origin. Because of all this, for an increase of one degree Celsius, the two media made up of the atmosphere and the UOS will have to absorb many more calories than their conventional heat capacity predicts. To take this into account, our model uses the concept of "dynamic heat capacity" introduced by Zeltz [12] and which makes it possible to integrate very briefly but really many phenomena:

- For the dynamic heat capacity of the UOS: currents, movements and mixing caused by winds, vertical convexions, rotation of the earth, thermal imbalance between high and low latitudes, cold water inputs caused by ice melting, proximity to the cooler thermocline immediately below the mixing layer, etc. It evolves in proportion to the volume of the UOS.
- For the dynamic heat capacity of the atmosphere: the thermal consequences of turbulence, vertical convection, mixing, various heat exchanges (latent heat linked to the condensation of water in clouds; sensible heat exchanges; radiation influences; proximity to the tropopause at a cold and constant temperature, etc.). On the other hand, we can notice that if GHGs increase, the greenhouse effect also increases and therefore the dynamic heat capacity of the atmosphere also increases. This aspect will be clarified later and will allow the model to integrate the different possible scenarios for future anthropogenic GHG emissions.

Model Description

Let us now specify the hypotheses, the notations used and the relationships that will intervene:
C_n denotes the amount of heat acquired or lost during month n by the UOS and θ_n its average temperature.

Similarly, the quantity of heat acquired or lost during month n by the atmosphere will be denoted T_n and tn its average temperature at the bottom of the atmosphere during month n.
tn and therefore T_n are subject to four influences:

During month n, the energy balance of the UOS corresponds to the difference between the energy received and the energy lost during this period. It translates to this equation:

$$(1): C_n = (100 - a_n)R_g - b_n R_g - Re_n - K_n - K'_n - \sigma_n lV_n$$

And similarly, that of the troposphere corresponds to this relationship:

$$(2): T_n = b_n R_g + Re_n + K_n + \sigma_n lV_n$$

The notations used in (1) and (2) and the relations that specify them are detailed in Table 1.

Table 1: Summary of the Relationships Founding the Model and Complementary Relationships

N°	Relations	What is at stake.	Values of constants, details and complementary relations
1	$C_n = (100 - a_n)R_g - b_n R_g - Re_n - K_n - K'_n - \sigma_n l V_n$	Energy balance of the UOS per m².	Rg : energy coming from the monthly global radiation of solar origin. Rg =340×3600×24×30 =881280000 J/m² According studies[18,19]
2	$T_n = b_n R_g + Re_n + K_n + \sigma_n l V_n$	Energy balance of the troposphere per m².	We will take the value of the latent heat around 15°C at atmospheric pressure : l = 2470 000 J/kg
3	$C_n = CD_n (\theta_{n+3} - \theta_{n+2})$	Heat received for a column of 1 m² by the UOS during month n. The lag between the variables Cn and θn takes into account the oceanic thermal inertia [20].	CD_n is the "dynamic heat capacity" of the UOS in month n. Concept introduced by Zeltz [12]. θ_n represents the average temperature of the UOS during month n.
4	$T_n = CD'_n (t_{n+1} - t_n)$	Heat received for a column of 1 m² by the troposphere during month n.	CD'_n is the "dynamic heat capacity" of the troposphere in month n. Concept introduced by Zeltz [12]. tn represents the average temperature of the troposphere during month n. $CD'_1 = (1/30) \times CD_1$ (relationship obtained by comparing the thermal capacities of UOS and troposphere)
5	$b_n R_g = \frac{1}{3}(100 - a_n)R_g$	Solar part absorbed Through the Atmosphere.	According Poitou [19].
6	$cl_{n+1} = cl_n + \beta(\theta_{n+1} - \theta_n)$	Evolution in % of the OC cl_n present over the oceans during month n	β= 1, value of the constant obtained by "calibrating" with the observed data from Eastman et al [21].
7	$a_n = \gamma \times (68 + cl_n) \times 0.01$	Atmospheric albedo.	γ= 0.44 measures the ratio of atmospheric albedo to OC coverage. Relation according [21-23], in particular formula (5a) [23]. See also 4.2.1(a) [24]. The number 68 that occurs in the previous relationship corresponds to an estimate of the average cloud cover in % between July 2002 and April 2015 (downloadable from the provided link[1] https://modis.gsfc.nasa.gov.
8	If $\theta_n \geq t_n$, $K_n = kT(\theta_n - t_n)$, If $\theta_n < t_n$, $K_n = k'T(\theta_n - t_n)$	Evolution of exchanges of sensible heat from the UOS to the troposphere.	Effusivities expressed in $JK^{-1} m^{-2} s^{-1/2}$: k = 6 k' = 1590 T=3600× 24×30 = 2 592 000 s.
9	$K'_n = \frac{\theta_n K'_1}{\theta_1 s_n}$	Evolution of exchanges UOS/ lower layers.	$K'_1 = 0.2 \times \sigma_1 l V_1$
10	$s_{n+1} = s_n + \mu(\theta_{n+1} - \theta_n)$	Evolution of stratification	μ = 5, value of the constant obtained by "calibrating" with the observed data from Li et al [25].
11	$Re_n = Ra_n - Rs_n$	Net infrared radiation retained in the troposphere	
12	$Rs_n = \alpha \times tn^4$	Infrared radiation emitted from the surface of UOS	By noting $\varepsilon = t_{n+1} - t_n$, we will use the approximation : $Rs_{n+1} \simeq Rs_n \left(1 + \frac{4\varepsilon}{t_n{}^4}\right)$
13	Ra_n	Infrared trapping by the troposphere	Specified in the section 3.
14	$V_n = V_1 \left(\frac{\theta_n}{\theta_1}\right)\left(\frac{t_n}{t_1}\right)$	Change in quantity of evaporated water (according Belarbi and Saighi) [26].	V_1 = 75 kg (approximate amount of water that evaporates over 1 month over an area of 1 m² of the ocean subjected to a surface temperature of 14°C and a pressure of 1 bar)
15	$E_n = lV_n$	Energy of vaporization	
16	$\sigma_n = -0{,}1t_n + 0{,}8 + 0{,}1\theta_n$	Share of vaporization energy taken in the UOS	Taking into account Albertson[27], relation proposed and justified by Zeltz [12].

17	$\Theta_{n+1} = \Theta_n + c(A_{n+1} - A_n)$	"Observed" temperature of the UOS	$\Theta_1 = 14°C$ A_n : global mean ocean heat anomaly in month n. c= 1/30[12].
18	$T_{an+1} = Ta_n + (B_{n+1} - B_n)$	"Observed" temperature of the troposphere	$Ta_1 = 14°C$ B_n : global mean atmospheric temperature anomaly in month n.
19	$S_{n+3} = S_{n+2} + \lambda(\theta_n - \theta_{n-1}) + L>Th$	Average sinking of the base of mixed layer	λ = 100, value of the constant obtained by "calibrating" with the observed data from Sallée et al[28]. L = 0.03m et Th = 2 × 10^7 J [14].
20	$CD_n = CD_1 \times \frac{L_1+S_n}{L_1}$	"dynamic heat capacity" of the UOS. Relationship that translates the evolution of CDn as a function of the volume of the mixed layer.	$CD_1 = 3.6 \times 10^{11}$ J/K (estimate obtained by "calibrating" the model with the observations) Taking into account Le Calvé L_1 = 125 m [20].
21	CD'_n	"dynamic heat capacity" of the troposphere	Specified in the section 3. $CD'_1 = (1/30) \times CD_1 = 1.2 \times 10^{10}$ J/K

Consideration by the Model of the Main Possible Scenarios

Model Assumptions about the Greenhouse Effect

Let's start by specifying how the greenhouse effect will be apprehended and the different assumptions that will be adopted by the model:

According to Dufresne, in clear skies, water vapor (H_2O) is responsible for about 60% of the greenhouse effect, carbon dioxide (CO_2) for 26%, ozone for 8%, and other GHGs (methane, nitrous oxide, etc.) for 6%. Since they alone account for more than 85% of the greenhouse effect, we will initially only take into account water vapour and carbon dioxide [29]. The mechanisms leading to this greenhouse effect are different for both: For water vapour, when its concentration increases, the absorption of infrared radiation increases accordingly, as well as the temperature of the atmosphere; this results in an increase in the power of radiation emitted by the atmosphere towards the Earth's surface, and consequently an increase in its temperature.

On the other hand, the absorptivity of CO_2 for infrared radiation hardly changes according to its concentration when it is above 300 ppm, which is largely the case in the current atmosphere (CO_2 concentration above 400 ppm). To justify the greenhouse effect caused by this gas, we follow the explanation given by Dufresne and schematized in Figure 2 taken from this article:

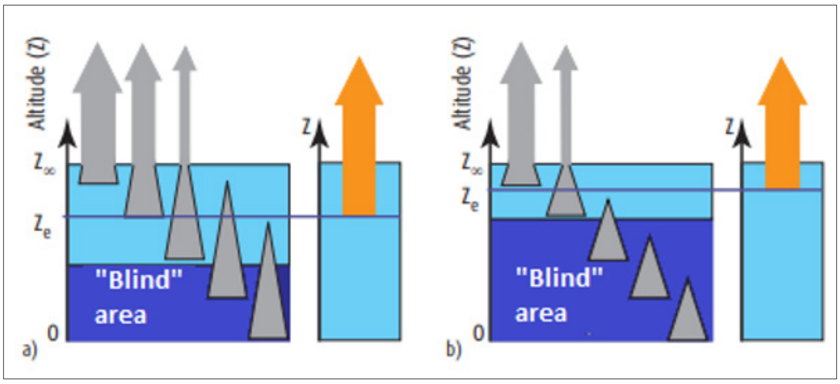

Figure 2: On the left, Schematic Representation of the Evolution of the Radiation Emitted upwards by the Surface and by the Atmosphere for 4 Particular Altitudes. The Surface is at Altitude 0 and the top of the Atmosphere at Altitude Z∞. The Triangle Shapes Schematize the Gradual Decrease in the Intensity of the Radiation with Altitude, due to Absorption by the Atmosphere, for Radiation Emitted at the base of the Triangle. On the Right, Representation of the Corresponding Emission Altitude. a) The Diagram Corresponds to a Reference Atmosphere; (b) The Diagram Corresponds to an Atmosphere for which the Quantity of Absorbent has Increased. Adapted from Dufresne and Treiner [29].

An increase in concentration mechanically leads to an increase in the emission altitude (height at which infrared rays are no longer trapped by GHGs and can escape into space).

And because of the negative temperature gradient, the heat received from the sun at the new emission altitude is no longer in equilibrium and causes the atmosphere to warm up, this warming then being transmitted to the surface of the globe. In the next section, we explain how we evaluate the CO_2 emission altitude as a function of its concentration.

Determination of the Emission Altitude

CO_2 in the Earth's atmosphere absorbs infrared radiation emitted from the Earth's surface, re-emitting some of this energy in all directions, including towards the Earth's surface. Figure 3 shows the variation in the infrared emissivity of CO_2 obtained for different temperatures thanks to Planck's law. Let us denote E(T) the emissivity of CO_2 at temperature T expressed in °K. From estimates of this emissivity, we obtain by the method of least squares: E(T) = 0.008T - 1.78.

According to Kirchhoff's law of radiation, the absorption and emission fluxes are identical for each frequency and direction. So, if we denote A(T) the average absorptivity of CO_2 at temperature T, we have: A(T) = E(T) = 0.008T - 1.78.

For the temperature, we will take a vertical gradient of -6.5°K per km altitude in the atmosphere (value in accordance with Dèléze for a standard humidity atmosphere) [30]. This negative gradient is independent of radiative exchanges and independent of CO_2 concentration. Taking the temperature at altitude 0: T(0)= 287°K (14°C), the temperature T(z) in degrees Kelvin at the altitude z expressed in meters is given by T(z)= 287 – 0.0065z.

For the density m(z) of the air expressed in kg/m³, from the data of Dèléze, we obtain by the method of least squares m(z)= -0.000038z + 1.198 [30].

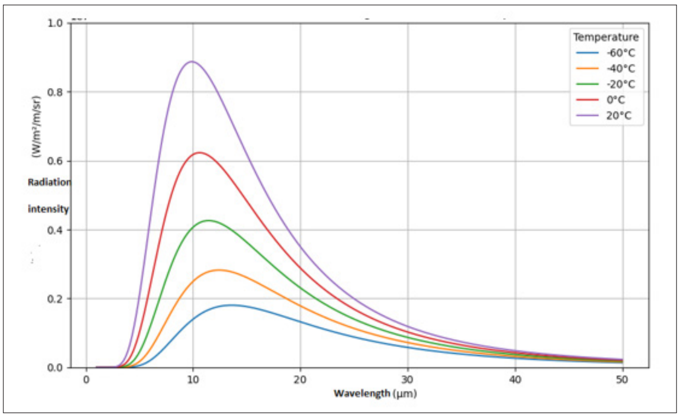

Figure 3: Variation of the Infrared Emissivity of CO_2 at Different Temperatures

Let z_n be the emission altitude for a $CO2_n$ concentration. The product $CO2_n \times m(z_n) \times E(T(z_n))$ is constant according to the variable n since it corresponds to the density of CO_2 where the latter can re-emit the infrared that it absorbs towards space. According to Dufresne the altitude of emission is between 3 and 8km. For 1950, when the CO_2 concentration was about 300ppm, we will assume (rather arbitrarily but taking into account the previous range) that the average CO_2 emission altitude was 5km [29].

Therefore
$CO2_n \times m(z_n) \times E(T(z_n)) = 300 \times m(5000) \times E(T(5000)) = 77.415$

Donc for any n, z_n is the solution of the equation $CO2_n \times m(z_n) \times E(T(z_n)) = 77.415$,
that is, the quadratic equation:
$1.976\times10^{-9}z^2 - 8.1904\times10^{-5}z + 0.61817 - (77.415/CO2_n) = 0$

This equation has two solutions, one giving a value that corresponds to a tropospheric altitude since it is located between 5000 and 10,000m, the other to stratospheric heights (more than 35,000m). The z_n emission altitude sought is therefore the first. Table 1 presents some CO_2 concentrations over the period 1955-2025 with their corresponding emission altitudes calculated by the previous method.

Table 1: CO_2 Concentrations Over the Historical Period 1955-2025 and Corresponding Emission Altitudes

Year	CO_2 concentrations (ppm)	Emission altitudes(m)
1958	315	5199
1960	316	5211
1970	325	5322
1980	339	5485
1990	354	5646
2000	369	5796
2006	381	5909
2013	396	6041
2014	398	6058
2015	400	6074
2016	403	6100
2017	405	6116
2018	407	6132
2020	413	6180
2021	420	6235
2023	424	6265

Determination of Ra_n

The Infrared trapping by the troposphere is defined by $Ra_n = R1a_n + R2a_n$ where R1an is the part coming from water vapour and $R2a_n$ is the part from the CO_2.

The model uses the recurrence relation $R1a_{n+1} = R1a_n \times \frac{v_{n+1}}{v_n}$ for the evolution of $R1a_n$.

Indeed, according to Loeb et al, the radiation retained by the greenhouse effect increases following in particular and above all the increase in evaporation caused by global warming [22]. To model $R2a_n$, we introduce the function f defined by

$$f(z_n) = CO2_n \int_0^{z_n} (m(z) \times E(T(z)))dz = CO2_n\,(6.5867\times10^{-10}z_n^3 - 4.0952\times10^{-5}z_n^2 + 0.61817z_n)$$

This function measures what is re-emitted as radiation in the zn height column by the CO_2

present there. We will therefore use the following relation:

$$R2a_{n+1} = R2a_n \times \frac{f(z_{n+1})}{f(z_n)}.$$

Following Poitou, we will take Ra1 = 340W/m² [19].

Since, according to Dufresne the contribution of water vapour is about 60%, we will take $R1a_1 = 204$W/m² and $R2a_1 = 136$W/m², a value that corresponds to the remaining 40% (26% for CO_2, 14% for the other GHGs) [29].

Apart from water vapour, our model therefore assimilates the other GHGs to CO_2.

Determination of CD'_n and Scenarios Considered for the Period 2025-2100

To determine CD'_n, we start from the following reasoning:

- When evaporation of oceanic origin V_n develops, $R1a_n$ increases, which accentuates the greenhouse effect, increases the atmospheric temperature and therefore also increases the capacity of the air to receive moisture and therefore heat (humid air has more heat capacity than dry air) and therefore this accentuates CD'_n.
- When the concentration of CO_2 in the atmosphere increases, the CO_2 emission altitude increases. So the part of the atmosphere directly affected by the greenhouse effect from CO_2 is increasing and so is CD'_n.

Hence the following relationship used by the model:

$$CD'_n = CD'_1 \times \frac{z_n}{z_1} \times \frac{V_n}{V_1}.$$

If we compare the thermal capacities of the troposphere and the UOS, the ratio is about 1 to 30, so we take $CD'_1 = (1/30) \times CD_1 = 1.2 \times 10^{10}$ J/K.

To evaluate $CO2\_n$ in the historical period 1955-2024, we will use data from Masson-Delmotte et al[31] and NOAA (downloadable from the provided link https://gml.noaa.gov/ccgg/trends/mlo.html).

For the future period 2025-2100 (n between 841 and 1754), we will consider four scenarios:

- **Scenario S1:** stabilisation of CO_2 emissions until 2030 and then a sharp gradual decrease. This scenario is quite comparable to what can be achieved under the Shared Socio-economic Pathways SSP 1 de study [31].
- **Scenario S2:** stabilization until 2040 and then a gradual decline that will return to a level of GHG emissions in 2100 close to that of the 1970-1980 decade. S2 can be obtained as part of SSP 2 [31].
- **Scenario S3:** The current increase stabilises until around 2060, then decreases very slightly to return to an emission level close to that of the decade 2000-2010 in 2100. S3 can be obtained as part of SSP 3 [31].
- **Scenario S4:** The current increase continues at the same rate and then ends up bending towards a slight decrease from 2080 onwards. S4 can be obtained as part of SSP 4 [31].

Figure 4 shows the graphs for the four scenarios considered.

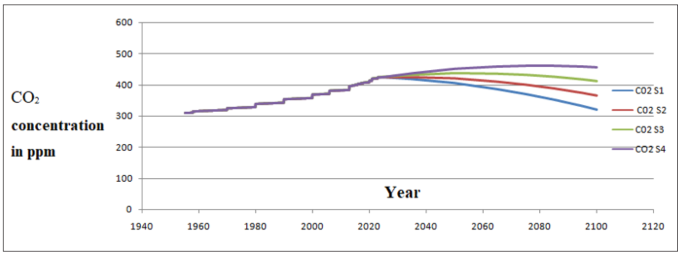

Figure 4: Evolution of CO_2 Concentration after 2025 Following Scenarios S1, S2, S3 and S4

We assume that there is a direct link between the additional CO_2 emissions and the CO_2 concentration of the atmosphere, which is quite approximate mainly for the following reasons:

- There is a certain inertia between the two phenomena. In addition, CO_2 has a long lifespan in the atmosphere. This implies that even if emissions were completely stopped, the concentration of CO_2 would only decrease slowly over time.
- Oceans, forests and other natural ecosystems absorb part of the CO_2 emitted on more or less long time scales (for example, concerning the absorption by the oceans, over several years or even several decades).
- The carbon cycle involves complex exchanges between the atmosphere, oceans, the terrestrial biosphere and sediments. And this introduces time lags between emissions and changes in atmospheric concentration.

Study of the Model

Theoretical Variations of the Five Parameters Taken into Account by the Model and a Quick Comparison with the Trends Projected by the GCMs

Table 2 presents the theoretical increases (i.e. without taking into account natural variability by the use of random coefficients) over the period 1955-2100 of the five parameters simulated by the model:

- The average temperature t_n at ground level (in °C).
- The average temperature θ_n of the UOS (in °C).
- The sinking S_n of the mixing layer (in m).
- The increase in oceanic stratification s_n (in %).
- The increase in the cloud cover cl_n (in %).

In the same order as these parameters, these theoretical increases are noted in the table Δ tt $\Delta\theta$t, ΔSt, Δst and Δclt.

Table 2: Theoretical Variations of the Five Parameters studied Over the Period 1955-2100

Scenario	Δtt (in°C)	Δ θt(in°C)	ΔSt (in m)	Δst (in%)	Δclt(in%)
S1	1.801	1.718	171.8	8.592	1.718
S2	1.818	1.717	171.7	8.588	1.717
S3	1.835	1.717	171.6	8.584	1.717
S3	1.850	1.716	171.5	8.580	1.716

We observe that the higher the CO_2 emissions in the scenario considered, the more Δtt increases. However, these increases are very small (only a few hundredths of a °C from one scenario to another). For the other four parameters, the variations observed between each scenario are almost insignificant. It follows that, according to the model, variations in CO_2 emissions or CO_2 equivalents do not seem to be a fundamental element in explaining the climate change observed since 1955. These results are very different from what is predicted as a trend for atmospheric temperature by the GCMs, which are much more sensitive to these scenarios. For example, concerning the increase in ground temperature for the period 1950-2100, Delmotte et al. predicts increases of around 1.4°C, 1.6°C, 2.7°C and 3.8°C for scenarios quite similar to S1, S2, S3 and S4 [31].

Asymptotic Behavior

Let's denote (t^t_n), (θ^t_n), (cl^t_n), (s^t_n), (a^t_n) and (S^t_n) the sequences "theoretical" (i.e. where natural variability is not taken into account by the model) from sequences (t_n), (θ_n), (cl_n), (s_n), (a_n) and (S_n). They verify the following proposition:

Proposition: The sequences (t^t_n), (θ^t_n), (cl^t_n), (s^t_n), (a^t_n) and (S^t_n) are strictly increasing and convergent.

Proof: Regarding what this proposal says about the (t^t_n), (θ^t_n), (cl^t_n), (s^t_n), (a^t_n) and (S^t_n), this has already been demonstrated in Zeltz[14], with the only difference that the dynamic heat capacities did not vary according to n but were assumed to be constant [13]. But the important point about them was that they were positive, which is still the case for CD_n and CD'_n. The only new point concerns the convergent growth of the suite (a^t_n). It stems from the relationship $a_n = \gamma\times(68+cl_n) \times 0.01$ and the already established convergent growth of the (cl^t_n).

For the rest, we will note t^t, θ^t, cl^t, s^t, a^t and S^t the finite limits of sequences (t^t_n), (θ^t_n), (cl^t_n), (s^t_n), (a^t_n) and (S^t_n).

Radiation Budget and Radiative Forcing from the Model

The radiation budget is the difference between the solar energy absorbed by the Earth (i.e. planet and atmosphere) and the energy radiated by the Earth to space.

Now $C_n + T_n$ corresponds to the difference between the energy received and the energy lost per m² of the "UOS + Atmosphere" system during month n. So to reach the monthly radiation balance br_n, just add the energy K'_n which dissipates towards the thermocline.
So $br_n = C_n + T_n + K'_n$

Now, according to lines 1, 2, 3 and 4 of Table 1, we have:
$C_n + T_n = (100 - a_n)Rg - K'_n = CD_n (\theta_{n+3} - \theta_{n+2}) + CD'_n (t_{n+1} - t_n)$
So $br_n = (100 - a_n)R_g = CD_n (\theta_{n+3} - \theta_{n+2}) + CD'_n (t_{n+1} - t_n) + K'_n$

Since the sequence (a^t_n) converges in increasing direction to at, the theoretical sequence (br^t_n) converges in decreasing direction to $br^t = (100 - a^t)Rg$. This indicates that according to our model, the climate system tends to approach a new thermal equilibrium where the incoming and outgoing energy are both equal to br^t.

The decreasing evolution of the theoretical thermal forcing can be evaluated in two ways:
Compared to br^t_1, by laying: $fr1^t_n = br^t_n - br^t_1$
Compared to br^t, by laying: $fr2^t_n = br^t - br^t_n = (a^t_n - a^t)R_g$
$fr1s^t_n$ and $fr2s^t_n$ defined by $fr1s^t_n = fr1^t_n /(30\times24\times3600)$ and $fr2s^t_n = fr2^t_n /(30\times24\times3600)$

make it possible to evaluate the theoretical evolution of average thermal forcings in W/m² from 1955 onwards.

Figure 5 (Figure 6) shows the changes in $fr1s^t_n$ (in $fr2s^t_n$) for the four scenarios, the differences between each of them are negligible. For the br^t evaluation needed for the calculation of $fr2s^t_n$, we have taken $br_{60,000} \approx br^t$

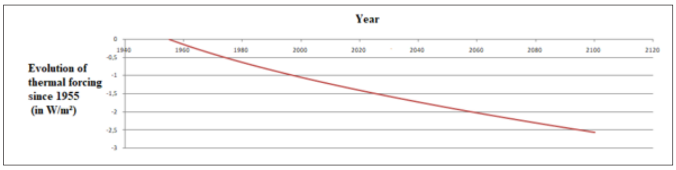

Figure 5 : Decrease in Thermal Forcing Since 1955 via $fr1^{st}_n$ (Scenarios S1, S2, S3 and S4)

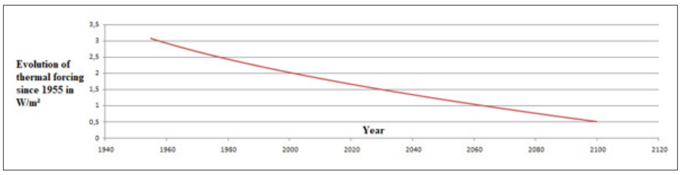

Figure 6: Decrease in Thermal Forcing Since 1955 via $fr2s^t_n$ (Scenarios S1, S2, S3 and S4)

The model therefore indicates that despite the "overheating" caused by GHG emissions, the thermal forcing decreases and tends towards 0.

Model Constant Testing

We performed several tests on the theoretical model to determine the relative importance that each constant or parameter can have to explain the warming observed since 1955 and its possible continuation after 2025 until 2100.

Test 1: We have set the model the initial emission rate of 1955 (about 310 ppm) throughout the period 1955-2100. As shown in Table 3, we find within a few thousandths the same values as those obtained in the context of the S1 scenario:

Table 3: Comparison Scenario S1 and Test « 310ppm »

Scenario	Δtt (in°C)	Δθt(in°C)	ΔSt (in m)	Δst (in%)	Δclt(in%)
S1	1.801	1.718	171.8	8.592	1.718
"310 ppm"	1.800	1.721	172.0	8.608	1.721

Test 2: We tested 2 values of λ, the coefficient that essentially determines the sinking of the mixing layer S_n (line 19 of Table 1): λ = 0 (no sinking regardless of the increase in the temperature of the UOS) and λ = 200, i.e. twice as much as the value 100 obtained by calibration with the observed data. Table 3 compares the three situations in the scenario S1:

Table 4: Testing on the Value of λ

λ	Δtt (in °C)	Δθt (in °C)	ΔSt (in m)	Δst (in %)	Δclt (in %)
λ = 100 (model)	1.801	1.718	171.8	8.592	1.718
λ = 0	2.937	2.832	0.12	14.162	2.832
λ = 200	1.458	1.388	277.4	6.940	1.388

There is a high sensitivity to this coefficient for all modelled climate parameters, and in particular temperatures.

Test 3: We also tested the γ coefficient that governs the evolution of atmospheric albedo a_n (line 7 of Table 1): γ = 0 (no atmospheric albedo effect, solar radiation reaches the ground entirely) and γ = 1 (the atmospheric albedo effect corresponds exactly to cloud cover). Table 5 allows us to compare with the case γ = 0.44 taken into account by the model to obtain for 1955 the value conventionally given in climatology for atmospheric albedo: 0.30.

Table 5: Testing on the Value of γ

γ	Δtt (in °C)	Δθt (in °C)	ΔSt (in m)	Δst (in %)	Δclt (in %)
γ = 0.44 (model)	1.801	1.718	171.8	8.592	1.718
γ = 0	2.325	2.212	221	11.062	2.212
γ = 1	0.991	0.959	95.8	4.795	0.959

Once again, we note a high sensitivity of the climate parameters in relation to this coefficient.

Test 4: Then we tested the β coefficient that governs the evolution of cloud cover cl_n (line 6 of Table 1): β = 0 (cl_n does not vary regardless of atmospheric temperature) and β = 10 (the variation of cl_n is then very sensitive to temperature increases). Table 6 allows us to compare with the case β = 1 taken into account to calibrate the model with the observations of low cloudiness reported by Eastman et al [21].

Table 6: Testing on the Value of β

β	Δtt (in °C)	Δθt (in °C)	ΔSt (in m)	Δst (in %)	Δclt (in %)
β =1(model)	1.801	1.718	171.8	8.592	1.718
β = 0	1.808	1.729	172.8	8.64	0
β =10	1.727	1.655	165.4	8.27	16.551

Apart from Δclt, of course, we see very little variation when β goes from 1 to 0. On the other hand, the large increase in cloudiness caused by the increase from 1 to 10 has significant repercussions on the other parameters. However, the values taken by β have a much smaller impact on them than with λ and γ.

Test 5: Finally, we tested the μ coefficient that governs the evolution of the s_n stratification (line 10 of Table 1): μ = 0 (s_n does not vary regardless of atmospheric temperature) and μ = 10 (the variation of s_n is then very sensitive to temperature increases). Table 7 allows a comparison to be made with the case μ = 5 taken into account to calibrate the model with the observations of oceanic stratification reported by Li et al [25].

Table 7: Testing on the Value of μ

μ	Δtt (in °C)	Δθt (in °C)	ΔSt (in m)	Δst (in %)	Δclt (in %)
μ =5 (model)	1.801	1.718	171.8	8.592	1.718
μ = 0	1.814	1.735	173.4	0	1.735
μ = 10	1.798	1.720	171.9	17.202	1.720

This time we see a very small impact on the other parameters.

In Table 8, we summarize the observations made in the previous tests using a scaled from 0 to 10 with 0 for no impact and 10 for a very strong impact:

Table 8: Impacts of the Coefficients on the Modelled Climate Parameters

coefficients	λ	γ	β	$CO2_n$	μ
impacts	9	7	5	1	1

Interpretation of Previous Tests

- The very large impact of λ on the parameters simulated by the model is consistent with the following fact: the heat capacity of the UOS is much greater than that of the troposphere above it and therefore in fact the climate is largely regulated by the mixing layer. The model is therefore fully in line with this very important aspect of the climate system.
- As we have earlier in this section, the radiation budget depends exclusively on the atmospheric albedo effect. So it is normal that for our model the γ coefficient that governs this albedo has a big impact on the simulated parameters.
- Cloud cover has direct effects on atmospheric albedo so it is consistent with the previous point that the β coefficient that governs cl_n also has a significant impact on the simulated parameters. This is also in line with the role played by low cloudiness: as has been robustly established in Zeltz [13], it has a function as a natural thermostat for the climate.
- The fact that variations in μ have very little impact on our model is explained by the fact that the sn stratification intervenes in our model only on the K'_n loss of heat from the UOS to the lower oceanic layers. This loss is in all cases low compared to the other energy flows that occur at all other levels.
- According to Table 1 (lines 2, 4, 5 and 11), we have:
- $t_{n+1} = t_n + \frac{H_n}{CD'_n}$ with $H_n = \frac{1}{3}(100 - a_n)R_g + Ra_n - Rs_n + K_n + \sigma_n l V_n$

Now CD'_n and $Ra_n = R1a_n + R2a_n$ are two increasing functions of the emission altitude zn and therefore also of $CO2_n$. So when $CO2_n$ increases, the growth of the term H_n is largely neutralized by that of CD'_n. This explains why in the end t^t_n varies very little when the CO_2 concentration increases. Since they are not directly dependent on $CO2_n$, the other modelled parameters θ^t_n, cl^t_n, s^t_n, and Stn are even less affected by CO_2 variations.

Simulation Examples

Figures 7 to 11 show simulations of the five parameters obtained by the model under the S1 scenario. For each of these simulations, the theoretical curve and the two curves limiting the 95% CI are added. These confidence intervals were obtained from point means and standard deviations from a series of 250 simulations.

As already noted in relation to the theoretical increases given in Table 2, there are very few differences with the other S2, S3 and S4 scenarios. So it seems unnecessary to us to add examples of simulations for these scenarios.

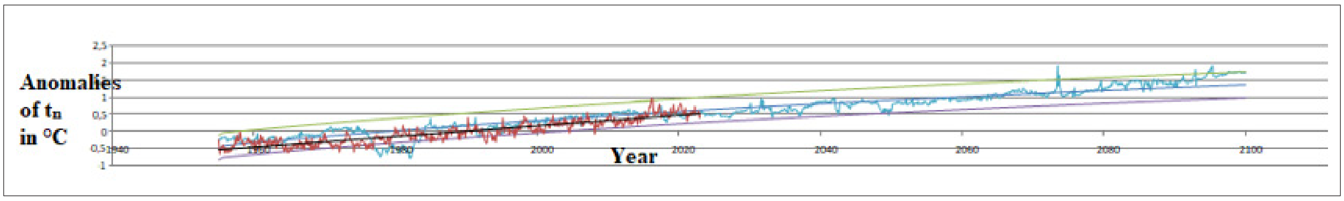

Figure 7: Simulations of Model for Atmospheric Temperature Anomalies in Scenario S1

Notes: Simulations of Stratification Anomalies s_n (red) and Observed Anomalies (blue) (in %). For other curves: the 95% Confidence Interval is Delimited by the Upper Curve and the Lower Curve. The Central Curve is the Theoretical Curve (without taking into Account Natural Variability) of s^t_n.

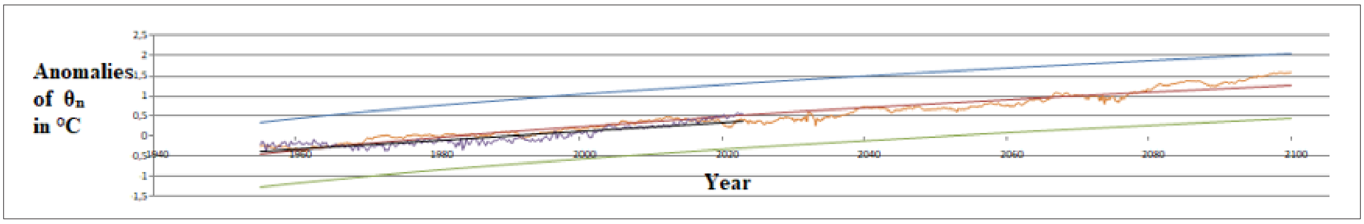

Figure 8: Simulations of Model for UOS Temperature Anomalies in Scenario S1

Notes: Simulations of UOS Temperature Anomalies θ_n (orange) and Observed Anomalies (purple) (in °C). For other curves: the 95% Confidence Interval is Delimited by the Upper Curve and the Lower Curve. The Central Curve is the Theoretical Curve (without taking into account Natural Variability) of θ^t_n.

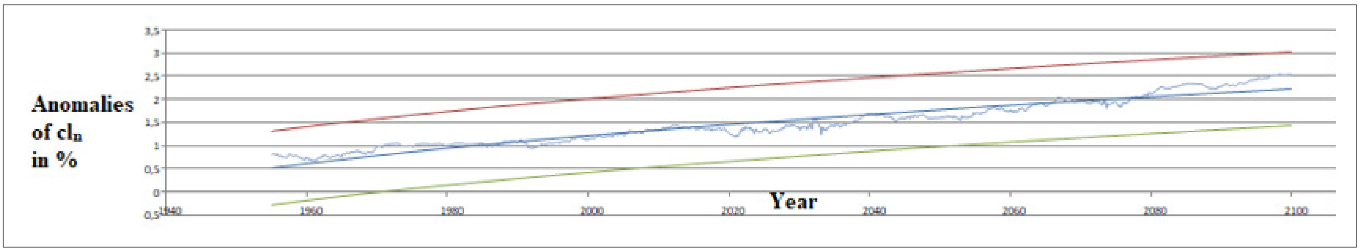

Figure 9: Simulations of Model for Cloud Cover Anomalies in Scenario S1

Notes: Simulations of Cloud Cover Anomalies cl_n (blue) (in %). For other Curves: the 95% Confidence Interval is Delimited by the Upper Curve and the Lower curve. The Central Curve is the Theoretical Curve (without taking into Account Natural Variability) of cl^t_n.

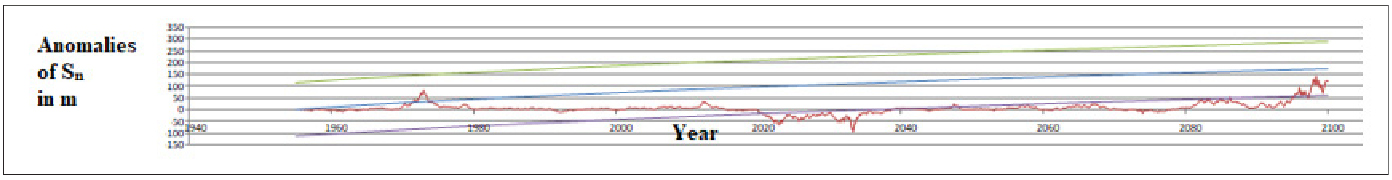

Figure 10: Simulations of Model for Sinking of the Mixing Layer Anomalies in Scenario S1

Notes: Simulations of Sinking Anomalies S_n (red) (in m). For other curves: the 95% Confidence interval is delimited by the upper curve and the lower curve. The Central Curve is the Theoretical Curve (without taking into account natural variability) of S^t_n.

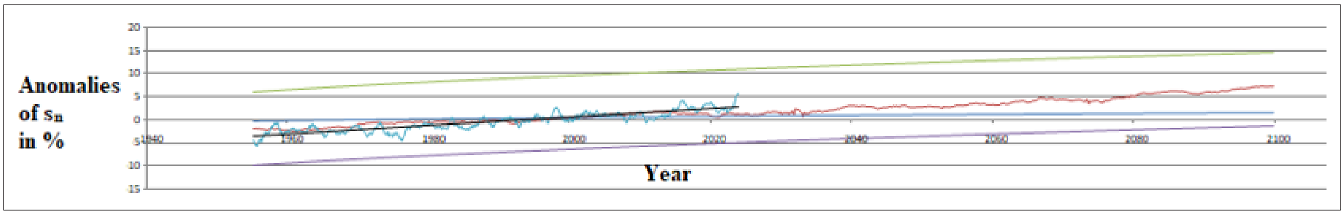

Figure 11: Simulations of Model for Stratification Anomalies in Scenario S1

Notes: Simulations of Stratification Anomalies s_n (red) and Observed Anomalies (blue) (in %). For other curves: the 95% Confidence Interval is Delimited by the Upper Curve and the Lower Curve. The Central Curve is the Theoretical Curve (without taking into Account Natural Variability) of s^t_n.

Connecting the Model Results with the Previous Period 1955

The concentration of CO_2 is estimated at 280 ppm during the pre-industrial era 1850-1900 (downloadable from the provided link ftp://aftp.cmdl.noaa.gov/products/trends/co2/co2_annmean_mlo.txt) period considered in relative radiative equilibrium. However, according to Schildknecht, up to a concentration of about 300 ppm, the atmosphere is not yet opaque to infrared radiation [32]. Thus, at the beginning of the industrial era, as the concentration of CO_2 in the atmosphere increased, its absorption by infrared rays also increased, which gradually caused and amplified an imbalance in the Earth's radiation budget. In 1955, when the concentration was about 310 ppm and with the high inertia involved in such phenomena, the atmosphere was still suffering the repercussions of this imbalance. As a result, the radiation balance, even if it was already decreasing, was still very marked in 1955.

What the Model Indicates about the Ergodicity Hypothesis

The future attainment, even remote, of a thermodynamic equilibrium is a strong argument in favour of an ergodicity of the climate system [33]. However, the mathematical proposition stated in this section clearly indicates that our modeling leads to a thermodynamic equilibrium. Similarly, the fact that it predicts a decrease in thermal forcing is consistent with the climate system ergodicity hypothesis.

Conclusion

If our model is realistic, and until proven otherwise , it is, it indicates that whatever the S1, S2, S3 or S4 scenario envisaged, the result in 2100 will be the same: at the 95% confidence level, an increase in atmospheric temperature over the period 1955-2100 of about 1.8 ± 0.4 °C. One could deduce a little quickly that the current efforts to reduce GHG emissions, especially CO_2, are completely useless. It is exactly the opposite, our model indicates that for these efforts to be useful, we must aim for a return to a CO_2 concentration below 300 ppm, therefore to an even greater effort than that leading to the S1 scenario, a fortiori to the S2, S3 and S4 scenarios. There, and only there, will the current thermodynamic equilibrium be broken and a new equilibrium will be established, this time towards a negative radiation balance, thus a tendency towards a cooling.

On the contrary, persisting in the scenarios envisaged would lead to "eternal" warming, even if according to our model its acceleration would tend towards 0.

Références

1. Roger Balian R (2017) Henri Poincaré's legacy in physics. Open addition journal http://journals.openedition.org/bibnum/1055.
2. Lorenz EN (1963) Deterministic Nonperiodic flow. J Atmos Sci 20: 130-141.
3. Moron V (2010) Climate models. ECCOREV days on modeling https://www.eccorev.fr/IMG/pdf/moron_mod2010.pdf.
4. Zeltz É (2025) New method for statistical analysis of climate time series. Environment and Resource 2 :15.
5. Vilani C (2002) Mean field limit. Cours de DEA, 2001-2002 https://cedricvillani.org/sites/dev/files/old_images/2013/03/champ-moyen.pdf.
6. Mischler S (2011) Introduction to mean-field limits for particle systems. https://cel.hal.science/cel-00576329/document.
7. Coudène Y (2012) Ergodic theory and dynamical systems. EDP https://laboutique.edpsciences.fr/produit/609/9782759809967/theorie-ergodique-et-systemes-dynamiques.
8. Rousseaux E, Voisin N (2007) Ergodic theory and applications. https://www.math.sciences.univ-nantes.fr/~wang/memoire-ter/TER_Theorie_Ergodique.pdf.
9. Ruelle D, Eckman JP (1985) Ergodic theory of chaos and strange attractors. Review of Modern Physisc 57: 617-656.
10. Robert R (2007) The butterfly effect no longer exists! https://inria.hal.science/hal-01350368.
11. Nicoud F. Mécanique des Fluides. Polytech Montpellier // IMAG - UMR CNRS 5149 https://imag.umontpellier.fr/~nicoud/Cours/MKFLU%20-%20turbulence.pdf.
12. Zeltz É (2023) Origins of "natural climatic nervousness" and its current accentuation. J Mod Green Energy https://hal.science/hal-04157619v1/document.
13. Zeltz É (2024) Analysis of the interaction of oceanic cloudiness with the upper oceanic stratum. J Inform Anal https://hal.science/hal-04562140v1/file/JIA20230420.pdf.
14. Zeltz É (2024) Mechanisms driving ocean stratification and mixed layer deepening. Explora Environ Resour 1: 4578.
15. Bréon FM (2025) Les modèles du climat sont-ils fiables? https://www.college-de-france.fr/fr/agenda/cours/changement-climatique-comment-sait-on-ce-que-on-sait/les-modeles-de-climat-sont-ils-fiables.
16. Levitus S, Antonov J, Boyer T (2012) World ocean heat content and thermosteric sea level change (0-2000m), 1955-2010. Geo Res Lett https://agupubs.onlinelibrary.wiley.com/doi/10.1029/2012GL051106.
17. Levitus S, Antonov J, Boyer T (2005) Warming of the world ocean, 1955-2003. Geo Res Lett 32: L02604.
18. Wild M, Ohmura A, Schär C (2017) The Global Energy Balance Archive (GEBA) version 2017: A database for worldwide measured surface energy fluxes. Earth Syst Sci Data 9: 601-613.
19. Poitou J.(2013) Composition atmosphérique et bilan radiatif https://www.refletsdelaphysique.fr/articles/refdp/pdf/2013/02/refdp201333p28.pdf

20. Le Calvé O (2025) Physical Properties of the Marine Environment. An Introductory Course in Physical Oceanography. Available from: https://www.yumpu.com/fr/document/ read/17123705/ proprietes-physiques-du-milieu-marin-olivier-le-calve.
21. Eastman R, Warren SG, Hahn CJ (2011) Variations in cloud cover and cloud types over the ocean from surface observations. J Climate 24: 5914-5934.
22. Loeb NG, Johnson GC, Thorsen TJ (2021) Satellite and ocean data reveal marked increase in Earth's heating rate. Geo Res Lett 48: e2021GL093047.
23. Wen G, Marshak A, Song W (2019) A relationship between blue and near-IR global spectral reflectance and the response of global average reflectance to change in cloud cover observed from EPIC. Earth Space Sci 6: 1416-1429.
24. Konsta D (2010) Evaluation of the description of clouds in climate models from satellite observations of the Atrain Atmospheric Sciences https://www.researchgate.net/publication/48907787_EVALUATION_DE_LA_DESCRIPTION_DES_NUAGES_DANS_LES_MODELES_DE_CLIMAT_A_PARTIR_DES_OBSERVATIONS_SATELLITALES_DE_L'A-TRAIN.
25. Li G, Cheng L, Zhu J (2020) Increasing ocean stratification over the past half-century. Nat Clim Change 10: 1116-1123.
26. Belarbi N, Saïghi MN (2007) Comparative study of methods for assessing the evaporation rate from a free water surface. Application to arid and semi-arid regions in Algeria https://hal.science/hal-00157582/document.
27. Albertson ML (2011) The mechanics of evaporation. La Houille Blanche 42 : 282-311.
28. Sallée JB, Pellichero V, Akhoudas C, (2021) Summertime increases in upper ocean stratification and mixed layer depth. Nature 591: 592-598.
29. Dufresne JL, Treiner J (2011) The Atmospheric Greenhouse Effect: More Subtle Than You Think! Meteorology 72: 31-41.
30. Délèze M. Pression atmosphérique en fonction de l'altitude. https://www.deleze.name/marcel/sec2/applmaths/pression-altitude/pression-altitude.pdf.
31. Masson Delmotte V, Zhai P, Pirani A (2021) Summary for Policymakers. In: Climate Change 2021 The Physical Science Basis https://www.ipcc.ch/report/ar6/wg1/.
32. Schildknecht D (2020) Saturation of the infrared absorption by carbon dioxide in the atmosphere. International Journal of Modern Physics https://www.worldscientific.com/doi/abs/10.1142/S0217979220502938.
33. Paillard D, Herbert C (2001) Climate dynamics and thermodynamics. LSCE - IPSL https://ceres.ens.psl.eu/IMG/Didier_Paillard_La_Rochelle(1).pdf.